Investigation on Flow Characteristics of SVC Nozzles

S. H. I. Jingwei[†], W. A. N. G. Zhanxue, Z. H. O. U. Li and S. U. N. Xiaolin

Collaborative Innovation Center for Advanced Aero-Engine, School of Power and Energy, Northwestern Polytechnical University, Xi'an, Shaan Xi Province, 710072, China

†*Corresponding Author Email: shijw@nwpu.edu.cn*

ABSTRACT

Shock vectoring control (SVC) is an important method of fluidic thrust vectoring (FTV) for aero-engine exhaust system. It behaves better on nozzle of high pressure ratio, and is considered as an alternative TV technology for a future aero-engine with high thrust-to-weight ratio. In this paper, the flow mechanism and vector performance, including the vector angle (δ_p) and thrust coefficient (C_{fg}), of 2D and axisymmetric SVC nozzles were investigated after the validation of turbulence models by experimental data. The influence of aerodynamic parameters, e.g. nozzle pressure ratio (NPR), secondary pressure ratio (SPR) and free-stream Ma number (M_∞) on flow characteristics and vector performance were studied numerically, and results show that unbalanced pressure distributions on nozzle internal walls determine δ_p, while shock waves dominate thrust loss, referring to C_{fg}. The "pressure release mechanism" of an axisymmetric SVC nozzle causes vector angle about 16.54% smaller than that of a 2D SVC nozzle at NPR of 6. The induced shock wave interacts with nozzle upper wall at SPR of 1.5, and results in the δ_p of a 2D SVC nozzle 12% smaller. A new parameter ($F_{y,modi}$) of side-force was redefined for free-stream conditions, taking the pressure distributions on nozzle external walls into account. Results indicate that pressure connection on nozzle external walls of an axisymmetric SVC nozzle causes vector performance better at $M_\infty > 0.3$ and the δ_p is about 11.2% larger at transonic conditions of M_∞ of 0.9 and 1.1.

NOMENCLATURE

A_9/A_8	nozzle expansion ratio
A_s/A_8	ratio of secondary injection area to nozzle throat area
C_{fg}	thrust coefficient
F_x	thrust along nozzle axis
F_y	thrust normal nozzle axis
$F_{y,modi}$	modified thrust normal nozzle axis
$F_{i.n}$	ideal thrust of nozzle
$F_{i.s}$	ideal thrust of secondary flow
κ	ratio of specific heat
L	length of nozzle
$L_{sep.}$	length of separation zone upstream of injection slot
$m_n.$	mass flow rate of nozzle
$m_s.$	mass flow rate of secondary flow
M_∞	ambient Mach number
NPR	nozzle pressure ratio
NPR_D	designed nozzle pressure ratio
P_{st}	ambient static pressure
P_9	static pressure of nozzle exit plane
P_0^*	total pressure of outer flow field
P_n^*	total pressure of nozzle inlet
P_s^*	total pressure of secondary inlet
R	ideal gas constant
SPR	secondary pressure ratio
SVC	shock vectoring control

T_{st}	ambient static temperature
T_n^*	total temperature of nozzle inlet
T_s^*	total temperature of secondary inlet
T_0^*	total temperature of outer flow-field
TV	thrust vectoring
W	width of a 2D SVC nozzle
W_s	width of injection slot
X_C	length of convergent section of nozzle
X_D	length of divergent section of nozzle
X_j	non-dimensional injection position on divergent section of nozzle
y^+	non-dimensional height of first grid near wall
β	nozzle divergent angle
θ	secondary injection angle
Θ	angle between Y direction and normal direction of nozzle outer wall
δ_p	Thrust vector angle,
τ	ratio of secondary flow total temperature to nozzle inlet total temperature
ω	ratio of secondary mass flow rate to nozzle mass flow rate
$\omega\sqrt{\tau}$	corrected flow ratio of secondary flow to primary flow

1. INTRODUCTION

Thrust vectoring (TV) technology offers enormous benefits to a fighter plane, e.g. enhancing agility and maneuverability at post-stall regime, improving survival rate and combat efficiency, shortening take-off and landing distance, and increasing stealth ability (Sehra, *et al.* 2004; Terrier, *et al.* 2003; Scharnhorst, 2013). It is becoming an absolutely necessary demand for a 4th and later fighter plane. Generally, there are two types of TV: mechanical TV and fluidic TV. Compared with the former one, fluidic TV has simpler structure, lower weight, and quicker vectoring response (Mason, *et al.* 2004). As reported by Deere (2003), using fluidic TV, 43-80% weight reduction, 7-12% improvement of engine thrust-to-weight ratio, and 37-53% reduction in nozzle procurement and life cycle costs was obtained. Therefore, fluidic TV technology is considered as an alternative TV technology for exhaust system of a future aero-engine and has been investigated worldwide.

Many concepts of fluidic TV have been proposed and investigated since 1990s, including co-flow TV, counter-flow TV, throat skewing (TS) TV, dual throat nozzle (DTN) TV and shock vectoring control (SVC) TV (Shih, *et al.* 1999; Deere, 2000; GU, *et al.* 2015). Wing (1994) studied a co-flow TV, based on the "Coanda effect", on a convergent-divergent nozzle experimentally. A vector angle (δ_p) of 8.7º was obtained at NPR of 2.0, and a conclusion that the method was invalid when NPR was larger than 4.0 was drawn. In the later investigations of Saghafi (2006) and HEO (2012), the co-flow TV method was adopted on a subsonic primary flow and a supersonic primary flow. They studied the flow mechanism of co-flow TV numerically and experimentally, and achieved a δ_p of 20º at NPR of 1.3 and 10º at NPR of 3.0, respectively. Strykoski and Krothapalli (1993) proposed "Counter-flow" TV which is characterized by counter flow and counter shear layer. The working principle, parameters affecting rules and usage range for subsonic and supersonic primary flows were identified, and the thrust vectoring efficiency of a δ_p of 8º per 1% suction secondary flow was obtained. Shi (2013) investigated jet attachment and control method numerically, and founded that a hysteresis phenomenon existed in the control course. Later, LIU (2014) concluded Ma number has magnificent influence on vector performance of a counter flow nozzle. In previous studies, it was also pointed out that problems e.g. the jet detachment control and efficient vacuum device restrict the usage of the method and are still needed to be solved. The idea of "throat skewing" method is manipulating sonic line using secondary injections at throat and divergent section to achieve primary flow deflecting. Catt and Miller (1995, 1999, 2001) investigated flow characteristics of a TS nozzle, obtained a δ_p of 8º, a thrust coefficient (C_{fg}) of 0.94 and a vector efficiency of 1.7-2.0º/% (that is vector angle of 1.7º-2.0º with per 1% secondary flow) at low NPR, but as studied by Zhang

(2012), the vector performance of TS method is lower than SVC method at higher NPR (NPR>6.24). The DTN TV involves a convergent–divergent nozzle (Deere, *et al.* 2005; Bellandi, *et al.* 2009). A vector angle is generated by injecting secondary flow upstream of throat which causes flow separation in the recessed cavity between the two geometric minimum areas. An efficient method to improve the thrust vectoring efficiency of a DTN was studied by GU (2015). The dynamic response of a DTN in open and closed-loop control was investigated numerically by Ferlauto (2016). As studied, this TV method works better at low and middle NPR conditions. The SVC method works as follow: injecting high pressure secondary flow into supersonic flow at a nozzle divergent section, inducing an oblique shock wave and generating side-force on nozzle walls to achieve thrust vectoring (Hamed, *et al.* 1997). The SVC method is characterized by transverse injection and shock / boundary layer interaction. Complex shock waves, vortices and shear layers are involved, and parameters e.g. shock wave structures, jet trajectory, injection penetration and flow separation types are focused and CHAI (2012) provided fitting formulas of jet trajectory with injection configurations and momentum ratio of secondary flow to primary flow. Zukoski (1964) proposed a blunt body theory in the study of injection penetration. The effect of secondary injection in supersonic flow is similar as a blunt body with a front surface of quarter sphere, and the penetration depth is the sphere radius. Counter rotating vortices upstream of injection slot and closed or open separation downstream of injection were witnessed inside a SVC nozzle. The restriction of nozzle walls and the effect of negative pressure gradient deforms shock surface and causes the interaction between a bow shock and nozzle wall at some conditions. Waithe and Deere (2003) showed that an SVC nozzle has vector efficiency of 0.8 º/%-2.2 º/% and C_{fg} of 0.86-0.94. Zhang (2012) concluded that SVC method is more suitable for large designed pressure ratio nozzle and a SVC nozzle could be an option for the exhaust system of a future aero-engine with high thrust-to-weight ratio. Due to the important advantages mentioned above, the SVC method was selected as the topic of the research.

Presently, two aspects of research work have been conducted on SVC method numerically and experimentally. One aspect is the study of complex flow mechanism and the influence of aerodynamic and geometric parameters, including NPR, SPR, secondary injection position, secondary injection angle, and inlet gases thermodynamic properties, on vector performance (Deere, 2000; Shi, *et al.* 2013, Zmijanovic, *et al.* 2014, HE, *et al.* 2017, Zmijanovic, *et al.* 2012,). They concluded that better thrust vectoring performance was obtained when the injection position moved afterward. An SVC nozzle with two injection slots performed better than an SVC nozzle with single slot at low pressure ratio, δ_p

improves by 50% with the increase of injection angle, thrust vectoring effectiveness decreases with increase of free stream Ma number, and gas molar mass has great effect on jet penetration and vector performance. The other aspect is multi-axis thrust vectoring exploration. Chiarelli and Wing (1993, 1994) combined SVC method and Coanda blowing method and achieved the thrust vectoring with pitch and yaw function. Giuliano (1994) conducted investigation on convergent- divergent nozzles with different flow path cross-sections and trailing-edge shapes at jet exit test facility and obtained multi-axis thrust vectoring control. Federspiel and Anderson (1995, 1997) investigated SVC/throat skewing combined concept and mechanical / fluidic concept and extended the usage of SVC method. In the perspective of design and application of an SVC nozzle, previous work provides useful conclusions and guidance.

In this paper, a practical comparison of a 2D SVC nozzle and an axisymmetric SVC nozzle was conducted, which would be helpful when choosing the SVC type for an aircraft. A series of quantitative research on the investigation of the differences of flow characteristics and vector performance between two types of SVC nozzles were carried out numerically, based on solving 3D Reynolds-averaged Navier–Stokes equations. Basic flow mechanism and the influence of critical aerodynamic parameters, including NPR, SPR and M_∞, were investigated. The vector angle and thrust coefficient were compared to evaluate performance differences. Especially, for the study of effect of M_∞, a new reasonable definition of side-force was proposed, taking the pressure distributions on nozzle outer wall into account. This work aims to improve understanding on an SVC nozzle.
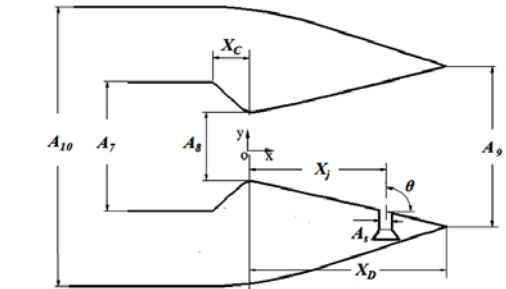
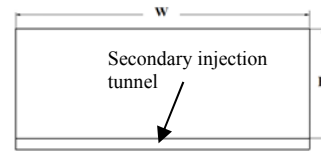## 2. NUMERICAL APPROACH

2.1 SVC Geometric Models

2D and axisymmetric SVC nozzles were investigated with same characteristic sizes, including nozzle inlet area (A_7), nozzle throat area (A_8), nozzle discharge area (A_9), nozzle convergent section length (X_C), nozzle divergent section length (X_D), nozzle length (L), secondary injection angle (θ), secondary injection position (X_j) and secondary injection area (A_s), which are shown in Fig. 1 and Table 1. And for the two types of SVC nozzles, the designed nozzle pressure ratio (NPR$_D$) is 13.88, while nozzle exit Ma number is 2.37. As seen in Fig. 1, the secondary injection slot of a 2D SVC nozzle has the same span-width with nozzle, and the injection slot of an axisymmetric SVC has a circular angle (ω) of 90º.
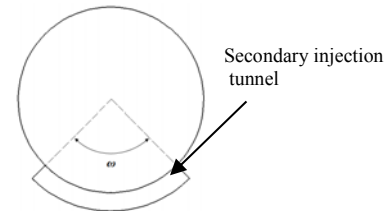
Table 1 Character parameters of SVC nozzles

A_9/A_8	X_D/L	NPR$_D$	A_s/A_8	X_j/X_D	θ (º)
2.33	0.829	13.88	0.0934	0.688	90

(a) Configuration of an SVC nozzle

(b) Injection section of a 2D SVC nozzle

(c) Injection section of an axisymmetric SVC nozzle

Fig. 1. Sketch of SVC nozzles.

2.2 Governing Equations

The numerical simulations have been carried out using Fluent of ANSYS 14.0. The flow characteristics were obtained by solving the compressible form of conservation equations continuity, momentum and energy equations in Cartesian coordinates, shown as follow:

Continuity:

$$\frac{\partial \rho}{\partial t} + \frac{\partial}{\partial x_i}(\rho u_i) = 0 \tag{1}$$

Momentum:

$$\frac{\partial}{\partial t}(\rho u_i) + \frac{\partial}{\partial x_i}(\rho u_i u_j) = -\frac{\partial p}{\partial x_i} + \frac{\partial \tau_{ij}}{\partial x_j} + \rho g_i + F_i \tag{2}$$

Energy:

$$\frac{\partial \rho E}{\partial t} + \frac{\partial}{\partial x_i}[u_i(\rho E + p)] = $$
$$\frac{\partial}{\partial x_i}[(\alpha + \frac{C_p \mu_t}{P_{rt}})\frac{\partial T}{\partial x_i} + u_j(\tau_{ij})_{eff}] \tag{3}$$

Where τ_{ij} is the shear stress tensor and is defined as follow:

$$(\tau_{ij})_{eff} = \mu_{eff}(\frac{\partial u_i}{\partial x_j} + \frac{\partial u_j}{\partial x_i}) - \frac{2}{3}\mu_{eff}\frac{\partial u_i}{\partial x_i}\delta_{ij} \tag{4}$$

The equations solved are the fully three-dimensional compressible Reynolds averaged

Navier-Stokes equations, which are discretized in finite volume form on each of the hexahedral control volumes. Second order upwind scheme is used in the spatial discretization, and second implicit scheme adopted for the time. The implicit density-based algorithm is used to solve the equation, and Roe averaged flux difference splitting (Roe-FDS) is chosen for the flux type.

2.3 Turbulence Model and Computational Grid

An SVC nozzle features transverse injection, and the applicability of turbulence model varies with working conditions, e.g. free stream Ma number, momentum ratio of secondary flow to primary flow et al. (Sriram, *et al.* 2004). In the section, experimental data of a 2D SVC nozzle from Deere (2000) was used to check the validation of turbulence models; the Spalart-Allmaras (*S-A*), Realizable κ-ε and shear stress transport (SST) κ-ω turbulence models were considered; and the predicted pressure distributions on nozzle wall are shown in Fig. 2. Compared with experimental data, the position of pressure abrupt increase (separation position of boundary layer upstream of injection slot) from *S-A* and Realizable κ-ε turbulence models lays behind experiment data, while SST κ-ω model offers well fitted results, and the error in separation position is less than 0.5%. Moreover, in high pressure zone upstream of injection slot and low pressure zone downstream of injection slot, SST κ-ω model behaves better, and the predicted error is within 2%. Therefore, the SST k-ω turbulence model with the compressible effect is selected for the study.
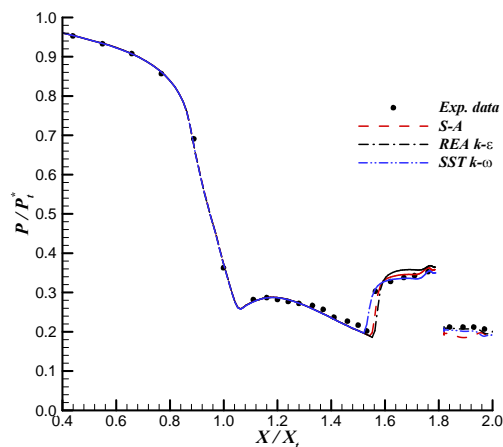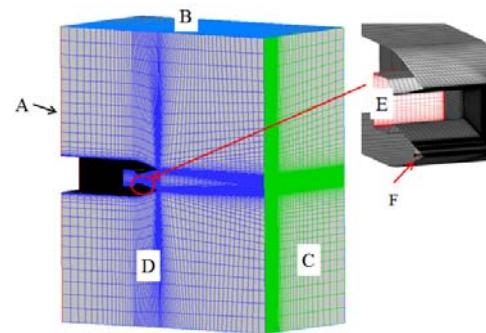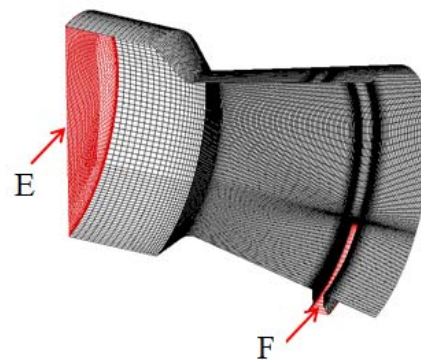

Fig. 2. Comparison on wall pressure distributions of computational and experimental data.

Then, a study on grid independence of the two SVC nozzles was conducted. Only half geometric models were used due to the symmetry of SVC nozzles, seen in Fig. 3. To satisfy the requirement of SST k-ω turbulence model on y^+ less than 5, the height of first grid above walls was carefully arranged. Totally, six grids were considered. They are 2.0 million, 2.8 million and 4.0 million cells for a 2D SVC nozzle and 1.5 million, 2.3 million and

3.4million cells for an axisymmtric SVC nozzle, respectively. The flow characteristics were focused on at the simulation condition of NPR of 13.88, SPR of 1.0 and free stream Ma number of 0.05. Pressure distributions along center line on nozzle down wall are shown in Fig. 4. The position and pressure are non-dimensionalized by length of nozzle divergent section and nozzle inlet total pressure, respectively. It is seen that for the two SVC nozzles the predicted results using coarse grid (grid #1 and grid #4) deviate a little from that of other grids. And results using middle grid (grid #2 and grid #3) and fine grid (grid #5 and grid #5) almost the same. It is concluded that results would not show differences when cell number exceed 2.8 million and 2.3 million for the two SVC nozzles respectively. Taking the calculation accuracy and time cost into account, the middle grids (grid #2 and grid #5) were selected to carry out the research work in this paper.

(a) A 2D SVC nozzle

(b) An axisymmetric SVC nozzle
A: Outer flow inlet, B: Pressure-far-field, C: Outlet, D: Symmetry, E: nozzle inlet, F: Secondary injection inlet

Fig. 3. Computational grid and boundary conditions.
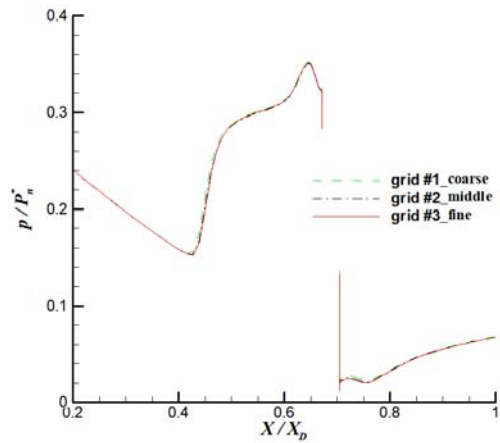
2.4 Boundary Conditions

Pressure inlet boundary is specified for nozzle inlet, secondary injection inlet and outer flow field inlet shown in Fig. 3, of which the total pressure (p_n^*, p_s^*, p_0^*), total temperature (T_n^*, T_s^*, T_0^*) and flow angle are prescribed. Nozzle pressure ratio varies from 6-16 while secondary pressure ratio has a range of 0.6, 0.8, 1.0, 1.2, and 1.5. 800 K is set for
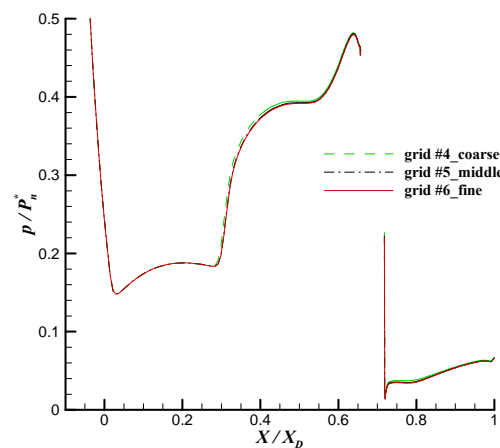
nozzle inlet total temperature, while Eq. (5) offers the total temperature of secondary inlet.

$$T_{s.}^* / T_0 = \left(P_{s.}^* / P_0 \right)^{\frac{\kappa}{\kappa-1}} \qquad (5)$$

On the outlet boundary, the static pressure (P_{st}) is imposed and the other variables are extrapolated from the interior. Symmetry boundary conditions are adopted at the center face. On pressure-far-field boundary, static pressure, free-stream M_∞ (0.05, 0.3, 0.5, 0.7, 0.9, 1.1 and 1.3) and flow direction are provided. Interior boundary including the nozzle exit and the secondary injection exit are monitored. Impermeable, no-slip and adiabatic wall boundaries are applied on the solid walls to ensure zero normal flux of mass, momentum and energy crossing the mesh face that lapped with the wall boundary.

(a) A 2D SVC nozzle

(b) An axisymmetric SVC nozzle

Fig. 4. Grid independence results for SVC nozzles.

2.5 Definitions of Performance Parameters

For SVC nozzles, two parameters are used to estimate their performance: the thrust vector angle (δ_p) and the thrust coefficient (C_{fg}). Their definitions are as follow:

$$\delta_p = \tan^{-1}(F_y / F_x) \qquad (6)$$

In the Eq. (6), F_x and F_y are components of thrust in X and Y direction respectively, and they are calculated from momentum equation, and in detail they are in Eq .(7) and Eq. (8).

$$F_x = \int_{A_9} (\rho v_x v_x + (p - p_0)) dA \qquad (7)$$

$$F_y = \int_{A_9} \rho v_x v_y dA \qquad (8)$$

Thrust coefficient is defined as the ratio of actual thrust to ideal thrust, seen in Eq. (9).

$$C_{fg} = F_{noz.} / (F_{i.noz.} + F_{i.sec.}) \qquad (9)$$

where $F_{noz.}$ is the actual thrust of a nozzle and is calculated by equation of $F_{noz.} = \sqrt{F_x^2 + F_y^2}$. $F_{i.noz.}$ and $F_{i.sec.}$ are the ideal thrust of primary flow and secondary flow, and they are obtained in Eq. (10) and Eq. (11), respectively:

$$F_{i.noz.} = m_{n.} \sqrt{\frac{2\kappa R}{\kappa-1}} \sqrt{T_n^*[1-(\frac{p_0}{P_n^*})^{\frac{\kappa-1}{\kappa}}]} \qquad (10)$$

$$F_{i.sec.} = m_{s.} \sqrt{\frac{2\kappa R}{\kappa-1}} \sqrt{T_s^*[1-(\frac{p_0}{P_{s.}^*})^{\frac{\kappa-1}{\kappa}}]} \qquad (11)$$

where κ is the ratio of specific heat.

Additionally, another critical parameter $\omega\sqrt{\tau}$ named as corrected flow ratio of secondary flow is defined (in Eq. (12)); it represents the momentum ratio of secondary flow to primary flow, and is critical to the separation length upstream of injection port and jet trajectory. Because the secondary flow is extracted from high pressure components of an aero-engine, there is a restriction on secondary flow rate. Generally, the value of $\omega\sqrt{\tau}$ should be within 0.15.

$$\omega\sqrt{\tau} = m_{s.}\sqrt{T_{s.}} / m_{n.}\sqrt{T_{n.}} \qquad (12)$$

where ω is the ratio of secondary mass flow rate to nozzle mass flow rate, and τ is the ratio of secondary flow total temperature to nozzle inlet total temperature.

3. RESULTS AND DISCUSSION

3.1 Flow Mechanism of SVC Nozzles

Flow characteristics (on symmetric plane) of a 2D SVC nozzle are shown in Fig. 5. When high pressure secondary flow is injected into supersonic primary flow of nozzle divergent section, strong interactions between injected jet and primary flow occur. A quasi-two-dimensional oblique shock wave, rooting from supersonic flow of boundary layer, is induced. The strength and angle of oblique shock wave are mainly affected by jet penetrating

depth which denotes jet disturbance degree and is associated with nozzle geometric parameters and corrected flow ratio of secondary flow ($\omega\sqrt{\tau}$). High pressure rise caused by induced shock wave brings out strong positive pressure gradient for local flow nearby nozzle wall, thickening boundary layer and even making boundary layer to separate. Then a cuneiform-like separation zone before injection slot is formed, and it interacts with induced shock wave, resulting in a "λ" shock wave system. Also shown in Fig. 4, the *Ma* number before "λ" shock wave is about 1.80-2.25, while that after "λ" shock wave is about 0.60-2.00. In one aspect, the shock wave loss here is the dominating loss source for an SVC nozzle, and it can cause a large reduction for nozzle thrust coefficient (C_{fg}). In another aspect, the "λ" shock wave leads to unbalanced pressure distributions on nozzle upper and lower walls (Fig. 6) and provides side-force for primary flow deflecting. Commonly the unbalanced pressure zone characterized is by length of high pressure zone ($L_{sep.}$) upstream of injection slot, which can illustrate vector performance of an SVC nozzle; and as is investigated, $L_{sep.}$ is mainly associated with $\omega\sqrt{\tau}$. From analysis on data of different working conditions, an approximate fitting equation can be obtained as follow.

$$L_{sep.} / w_{s.} = 7.493 + 2.234\omega\sqrt{\tau} + 2.7596(\omega\sqrt{\tau})^2 \quad (13)$$
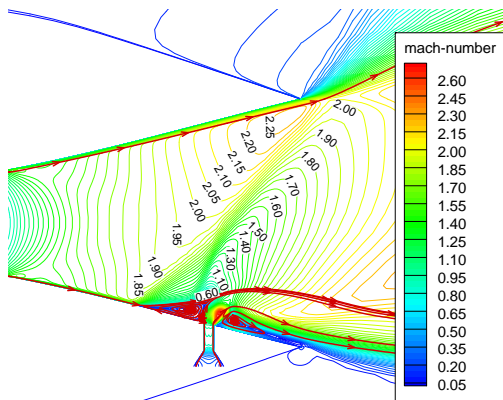

Fig. 5. Flow field on the symmetric plane of a 2D SVC nozzle (NPR=13.88, SPR=1.0).

Besides, upstream and downstream of injection slot, complex flow separating and vortex system exist. A pair of counter-rotating vortices can be witnessed upstream of injection slot; they are formed by boundary layer separation and jet entrainment, respectively. And the dividing line of the two vortices lays on the position of peak pressure (seen in Fig. 6). Open or close separation appears downstream of injection slot under different working conditions; when $\omega\sqrt{\tau}$ is less than 0.088, injected jet reattaches nozzle lower wall, there is a close separation bubble, Otherwise, open separation would show up, and ambient air out of an SVC nozzle will be entrained into the separation zone. Also flow unsteadiness can be caused by open separation; the jet trajectory, shock wave position,

pressure distribution and vector angle will be affected. Results show that, from fast Fourier transform (FFT) of monitored pressure, maximal pressure amplitude of 4.05 kPa is obtained; and for the vector angle, a fluctuation within 2% is observed.
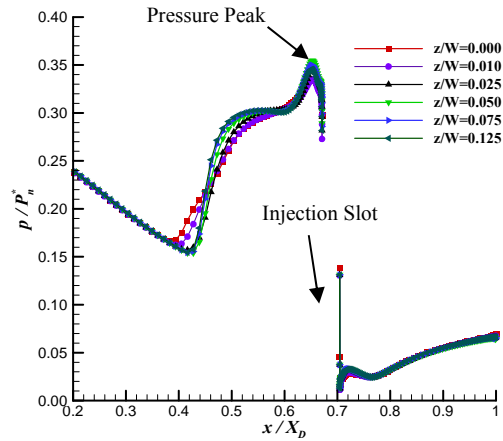

Fig. 6. Pressure distributions on nozzle lower wall of different z positions (NPR=13.88, SPR=1.0).
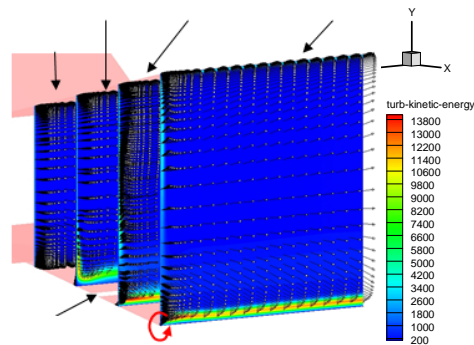

Fig. 7. Turbulent kinetic energy distributions on different sections (NPR=13.88, SPR=1.0).

Though, a 2D SVC nozzle is characterized by two dimensional flow pattern, three dimensional effects are also clear near side walls. Figure 6 shows the longitude pressure distribution of different span-wise position (Z direction); the X coordinate is non-dimensionalized by nozzle divergent section length (L_D), while the Y coordinate is non-dimensionalized by total pressure of nozzle inlet. As can be seen, the boundary layer separation positions of z/W of 0.01 and 0.02 are slight ahead of others', but when z/W is larger than 0.025, the separation positions of boundary layer are coincident. The three dimensional effect is associated with the merger of boundary layers on side wall and lower wall of an SVC nozzle. And this causes the low energy zone to increase, which weakens the resistance ability of boundary layer on positive pressure gradient. Thus flow near sidewall separates earlier. The turbulent kinetic distribution of different X sections shows the influence of shock wave on sidewall, seen in Fig. 7; it can represents the increase on thickness of boundary layer on sidewall, which also brings out flow loss. Additionally, at the corner of sidewall

and lower wall, another three dimensional effect can be seen. A stream-wise vortex (seen in Fig. 7) is caused by high pressure from jet and low pressure from separated flow downstream of injection slot. It affects the diffusion of nozzle exhausting gas which has high temperature and high species concentration, and eventually reduces the infrared radiation intensity of SVC nozzle by 35%-50% at some high observation angles.
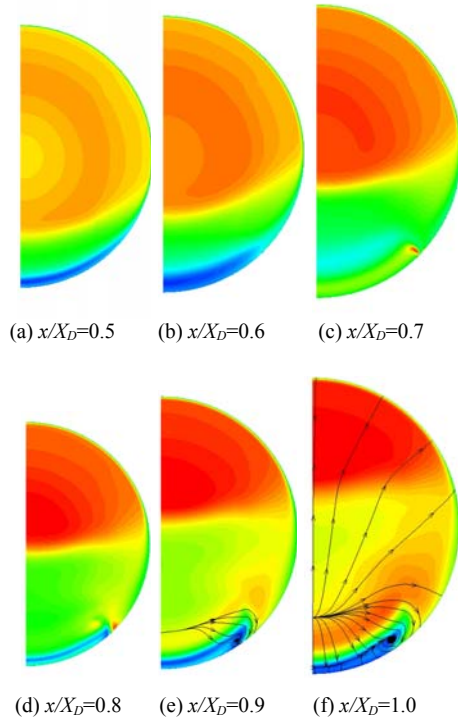

(a) x/X_D=0.5   (b) x/X_D=0.6   (c) x/X_D=0.7

(d) x/X_D=0.8   (e) x/X_D=0.9   (f) x/X_D=1.0

Fig. 8. Flow characteristics of an axisymmetric SVC nozzle (NPR=13.88, SPR=1.0).

As for an axisymmetric SVC nozzle, the basic working principle is similar with a 2D SVC nozzle, however, the flow characteristics are dominated by three dimensional flow pattern, and they are seen in Fig. 8 which show the *Ma* number distributions on different X sections (x/X_D = 0.5, 0.6, 0.7, 0.8, 0.9, and 1.0); the shock wave is a curved surface which can be identified by discontinuity of flow-field on X sections, while the separation line of boundary layer is a spatial curved line (convergent limited streamline seen in Fig. 9 (a)). Moreover, compared with a 2D SVC nozzle, the secondary injection slot of an axisymmetric SVC nozzle is not restricted by nozzle walls in span-wise direction, and it changes the configurations of vortices, especially for those near injection slot. As can be seen in Figs. 8 and 9, positive gradient between high pressure zone upstream of injection slot and low pressure zone downstream of injection slot accelerates local flow and induces vortices. The labeled local high speed flow (in Figs. 8 (c), (d) and (e)) is from separated boundary layer upstream of injection slot and outer layer of boundary layer, goes by injection slot and develops into flow with stream-wise vortex (in Fig. 9 (c)) and it is also benefits for the reduction of infrared radiation intensity of an SVC nozzle.

Meanwhile low speed flow goes around injection slot into low pressure zone after injection slot, forming a Y direction vortex (seen in Fig. 9 (a) and (b)); it plays a role of balancing pressure distributions, in another word, it connects the high pressure zone upstream of injection slot and low pressure zone downstream of injection slot, and this is also called "pressure release mechanism" which affects vector performance under some working conditions and causes differences from a 2D SVC nozzle.
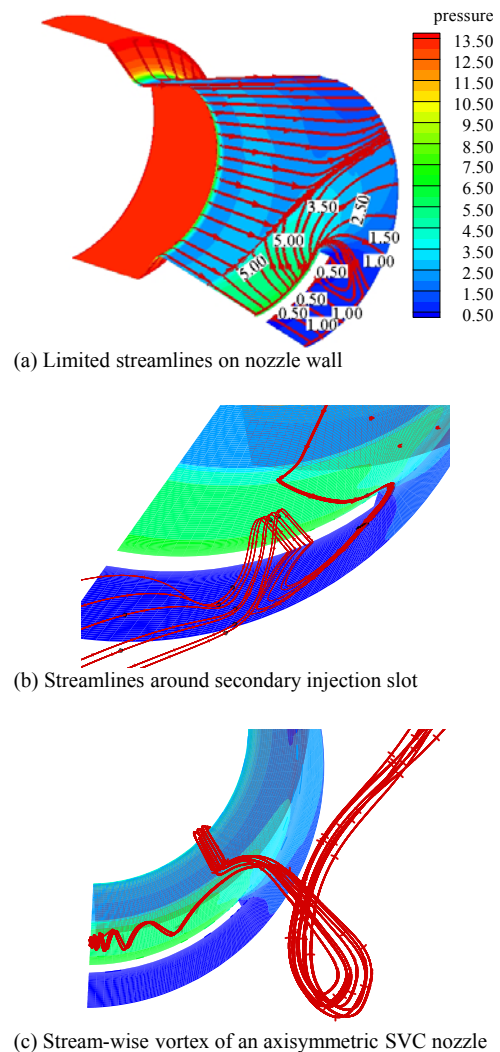

(a) Limited streamlines on nozzle wall

(b) Streamlines around secondary injection slot

(c) Stream-wise vortex of an axisymmetric SVC nozzle

Fig. 9. Flow characteristics of an axisymmetric SVC nozzle (NPR=13.88, SPR=1.0).

3.2 Influence of NPR on Vector Performance of SVC Nozzles

The influence of nozzle pressure ratio (NPR) on vector performance is due to the variation of nozzle wall pressure distributions caused by shock wave and flow separation. Generally, under different working conditions, the high pressure zone upstream of injection slot and low pressure zone downstream of injection slot are two main affecting zones. When NPR varies, the corrected flow ratio of secondary flow ($\omega\sqrt{\tau}$) keeps almost unchanged

(the variation of $\omega\sqrt{\tau}$ is within 1%). According to Eq. (9), the zone of high pressure upstream of injection slot is also unchanged. However, for the low pressure zone downstream of injection slot, static pressure on nozzle wall, which is non-dimensionalized by nozzle inlet total pressure, shows obvious variation, seen in Fig. 10; with the decrease of NPR, the local non-dimensional wall pressure increases from about 0.06 to 0.14, and this makes the efficient non-dimensional side-fore to ascend, resulting in higher vector angle (δ_p). Seen in Fig. 11, comparing the δ_p of different NPR conditions, about 85.71% and 56.20% increase in δ_p are obtained when NPR decreases from 16 to 6 for a 2D SVC nozzle and an axisymmetric SVC nozzle respectively.
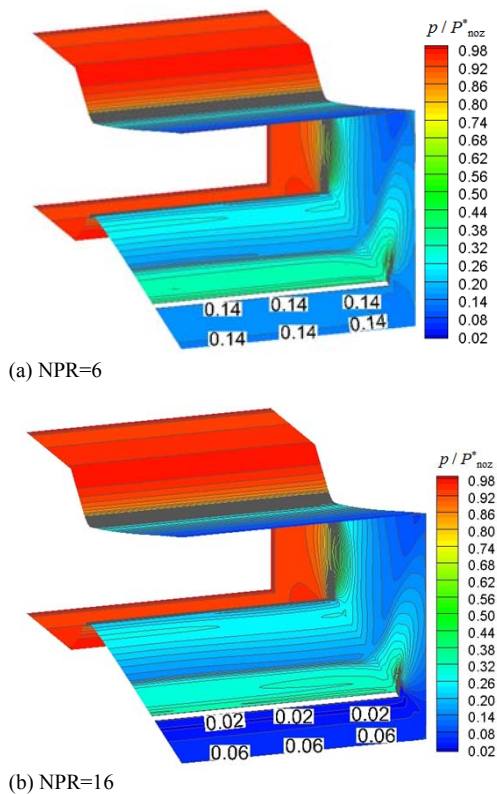

(a) NPR=6

(b) NPR=16

Fig. 10. Pressure distributions on down wall of a 2D SVC nozzle.

Noticeably, when SVC nozzles work at designed nozzle pressure ratio (NPR$_D$ of 13.88), the δ_p of two nozzles is nearly the same. At the condition, $\omega\sqrt{\tau}$ of an axisymmetric SVC nozzle is about 2.0% higher than that of a 2D SVC nozzle, which is associated with the configuration of injection slot and is benefit for vector angles. However, the high pressure before injection slot of axisymmetric SVC nozzle is not restricted and it causes vector efficiency a litter smaller; this is a critical affecting factor, especially for nozzles at over-expansion conditions. As can be seen in Fig. 11, with the decrease of NPR, the difference between δ_p of two nozzles increases; at the condition of NPR of 6, the δ_p of a 2D SVC nozzle is 14.88º, while that of an axisymmetric SVC nozzle is 12.76º and it is about 16.54% smaller. At under-expansion condition

(NPR of 16), the effect of "pressure release mechanism" weakens, and due that the $\omega\sqrt{\tau}$ of an axisymmetric SVC nozzle is 2% larger. Consequently, the δ_p is about 1.67% larger.
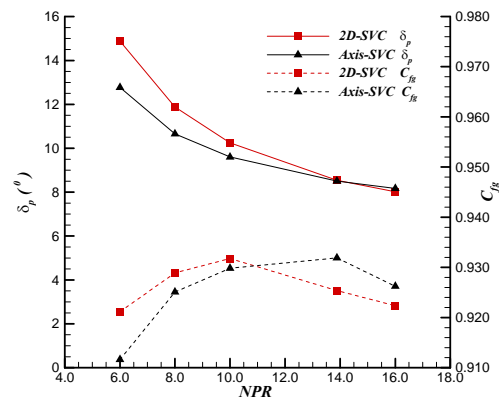

Fig. 11. Variation of vector angle and thrust coefficient with NPR (SPR=1.0).

For the flow loss of SVC nozzles, it includes shock wave loss, separation loss and friction loss, among which shock wave loss dominates. From Fig. 11, it can be seen, the thrust coefficients (C_{fg}) of two SVC nozzles are about from 0.910 to 0.932; the maximal C_{fg} of 0.931 and 0.932 are achieved at NPR of 10 and 13.88 respectively for 2D and axisymmetric SVC nozzles. And this is related with the induced shock wave, for a 2D SVC nozzle, it increases static pressure of primary flow and counteracts the thrust loss caused by over-expansion partly, which is not obvious for an axisymmetric SVC nozzle. Therefore, the maximal C_{fg} of a 2D SVC nozzle is obtained at over-expansion condition, while that of an axisymmetric SVC nozzle is achieved at designed pressure condition. When NPR is less than 10, the C_{fg} of a 2D SVC nozzle is larger; at NPR of 6 and 8, the increment are 1% and 0.5% respectively. But when NPR is larger than 10, the C_{fg} of a 2D SVC nozzle is smaller by 1.3% and 0.6% for NPR of 13.88 and 16 respectively.

3.3 Influence of SPR on Vector Performance of SVC Nozzles

With the increase of secondary pressure ratio (SPR), the corrected flow ratio of secondary flow ($\omega\sqrt{\tau}$) and momentum ratio of secondary flow to primary flow ascend, which enhances the interactions between injected jet and primary flow and enlarges the jet penetration depth. Therefore, the angle of shock wave increases, the position of shock wave moves forwards, and it makes the boundary layer separating zone (the high pressure zone) upstream of injection slot to increase and results in larger side-fore for primary flow deflecting. Fig.12 (a) and (b) shows the limited streamline and pressure distribution wall of an axisymmetric SVC nozzle; it can be seen that the high pressure zone caused by induced shock wave grows substantially from SPR of 0.6 to 1.5, correspondingly the vector angle (δ_p) grows from 5.04º to 12.16º. It is concluded that the SPR is a key

controlling parameter for SVC nozzles.

(a) *SPR*=0.6, an axisymmetric SVC nozzle

(b) *SPR*=1.5, an axisymmetric SVC nozzle
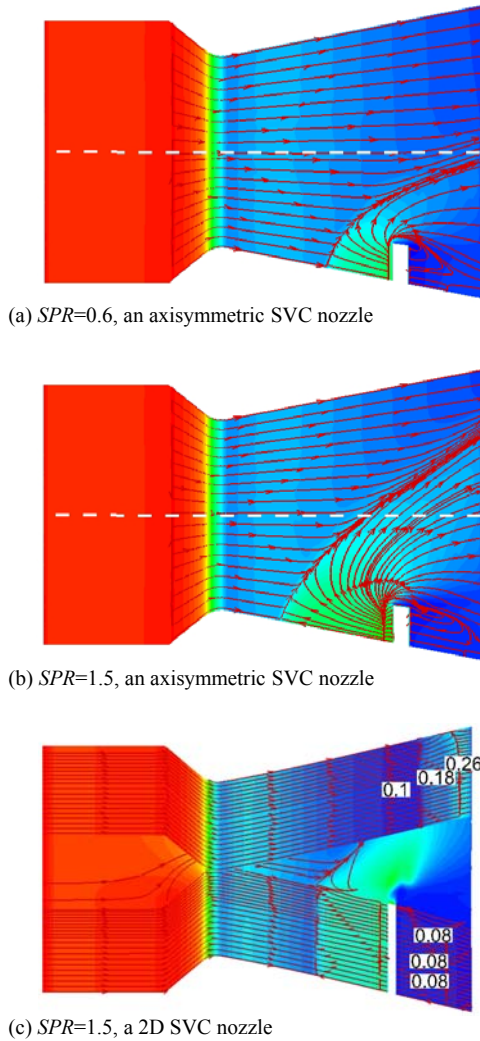

(c) *SPR*=1.5, a 2D SVC nozzle
Fig. 12. Limited streamlines and pressure distributions on SVC nozzle wall (NPR=13.88).

Shown in Fig.13, the variation of δ_p with different SPRs under designed nozzle pressure ratio (NPR$_D$ of 13.88), the difference between δ_p of a 2D and an axisymmetric SVC nozzle is within 1% when SPR is less than 1.0; however when SPR increases from 1.0 to 1.5, δ_p of the two SVC nozzles become to 10.84º and 12.16º respectively, and the δ_p of a 2D SVC nozzle is 12% less than that of an axisymmetric SVC nozzle. This is mainly because of the spatial position of induced shock wave; for a 2D SVC nozzle, when SPR is larger than 1.0, the induced shock wave gradually comes close to the upper wall of nozzle, and interacts with it at SPR of 1.5. Seen in Fig.12 (c), the induced shock wave causes closed separation of boundary layer on upper wall, makes local non-dimensional pressure to increase abruptly from 0.10 to about 0.26, and finally reduces the total side-fore of primary flow, weakening the augment of δ_p obviously. But for an axisymmetric SVC nozzle, at the condition of SPR of 1.5, although the high pressure zone goes beyond the center line (dashed line in Fig. 12 (b)) to the

upper zone, its influence on side-fore and vector performance is gentle, so is it on δ_p.

Comparing the thrust coefficient (C_{fg}) of the two SVC nozzles, it is obtained in Fig. 13, the C_{fg} of an axisymmetric SVC nozzle is always higher than that of 2D SVC nozzle; at smaller SPRs of 0.6 and 0.8, the differences between them are about 0.3%; while SPR are 1.0, 1.2 and 1.5, the differences are 1.17%, 0.89% and 0.76% respectively. The larger shock wave loss of a 2D SVC nozzle is the main affecting reason. As is discussed in last passage, the shock wave is more close to upper wall of 2D SVC nozzle, and more primary flow go through it, therefore larger loss is generated. So a conclusion can be drawn that at designed nozzle pressure condition or nozzle under-expansion conditions, the performance of axisymmetric SVC nozzle is better than that of 2D SVC nozzle over wide range of SPRs.
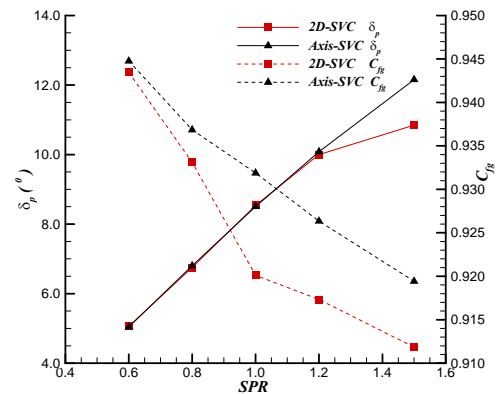

Fig. 13. Variation of vector angle and thrust coefficient with SPRs (NPR=13.88).

3.4 Influence of Free Stream Ma Number on Vector Performance of SVC Nozzle

Free stream Ma number (M_∞) has effects on subsonic zones of nozzle internal flows, e.g. separation zone downstream of injection slot and boundary layer on nozzle upper wall, and has effect on pressure distributions of nozzle outer wall. As is investigated, the former factor can be neglected, while the later one changes total side-fore of SVC nozzle and varies with M_∞. In order to estimate influence of M_∞ on vector performance of SVC nozzles, the side-force (F_y) should be redefined. Taking the unbalanced pressure on nozzle outer wall into account, the modified side-force $F_{y.modi}$ is calculated as follow:

$$F_{y.\text{modi}} = \int_{A_9} \rho v_x v_y dA + \int_9^{10} (p - p_0)\cos\Theta dA \qquad (14)$$

In the secondary term of Eq. (10), 9 and 10 represent the position of nozzle exit and the position of maximal section of nozzle outer wall respectively, and Θ is angle between Y direction and the normal direction of nozzle outer wall.

When M_∞ is larger than 0.5, flow separation on

nozzle outer wall appears, seen in Fig. 14, and separation zone is larger on upper wall than that on lower wall; this is due to the impact of free stream and primary flow, which also causes larger pressure on upper wall than that on lower wall. Therefore the unbalanced pressure on nozzle outer wall is generated, and eventually it weakens the total side-force and vector performance of SVC nozzles. Additionally, with the increase M_∞, separation zone on nozzle outer wall enlarges and achieves maximal value at transonic condition of M_∞ of 0.9 and 1.3, seen in Figs. 14(b), (c), (f) and (g), consequently, the largest decrease on vector angles (δ_p) can be witnessed; compared the condition of M_∞ of 0.3 and 1.1, δ_p decreases from 8.26º and 8.39º to 7.10º and 7.89º for 2D and axisymmetric SVC nozzles. When M_∞ excesses 1.1 to 1.3, the separation zone on nozzle outer wall gradually reduces and the δ_p can have an increase of about 1.0-2.0% for the two SVC nozzles.
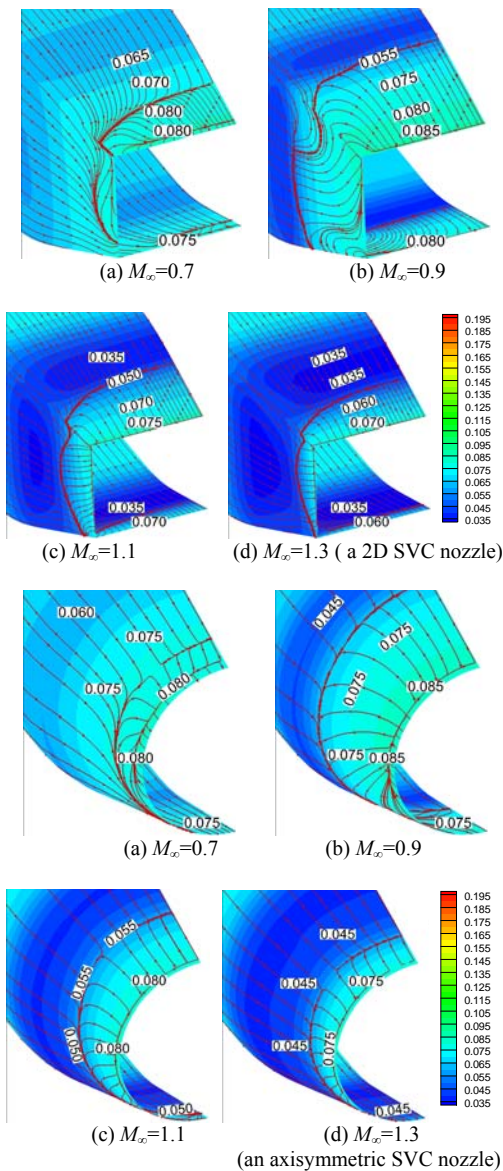

(a) M_∞=0.7   (b) M_∞=0.9

(c) M_∞=1.1   (d) M_∞=1.3 (a 2D SVC nozzle)

(a) M_∞=0.7   (b) M_∞=0.9

(c) M_∞=1.1   (d) M_∞=1.3 (an axisymmetric SVC nozzle)

Fig. 14. Limited streamlines and pressure distributions on SVC nozzle outer walls under different M_∞ (NPR=13.88, SPR=1.0).

Vector performance comparisons of two SVC nozzles are shown in Fig. 15. It is clear that M_∞ has the same affecting principle on δ_p, but the affecting level is different. This is caused by the configurations of nozzle outer walls; for a 2D SVC nozzle, the rectangular section can prevent the connection of the high pressure on upper wall and low pressure on lower wall, therefore larger separation zones and larger unbalanced pressure distributions are formed, seen in Fig. 14, and the decrease on δ_p is more obvious. Noticeably, at M_∞ of 1.1, the maximal difference on δ_p between 2D and axisymmetric SVC nozzles is obtained, and it is about 11.2%. Thrust coefficient (C_{fg}) of SVC nozzles represents the nozzle internal performance, so the unmodified side-fore is still used to calculate actual thrust of SVC nozzles. Seen in Fig. 15, the variation of C_{fg} with M_∞ is within 0.2% and the C_{fg} of an axisymmetric SVC nozzle is about 0.8% than that of a 2D SVC nozzle. And in summary, the axisymmetric SVC nozzle has better vector performance than 2D SVC nozzle under different M_∞ conditions.
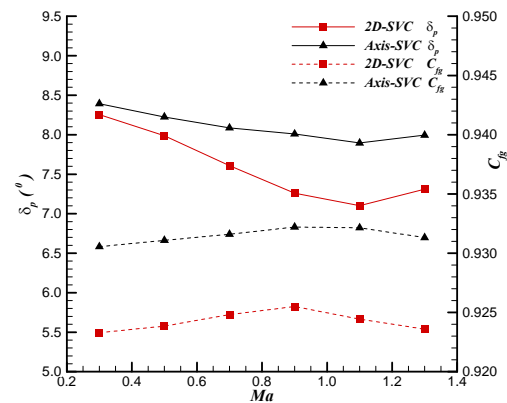

Fig. 15. Variation of vector angle and thrust coefficient with M_∞ (NPR=13.88, SPR=1.0).

In this paper, flow characteristics and vector performance of different SVC nozzles were studied based on CFD. The accuracy of simulation results was guaranteed by comparing predicted results from the chosen numerical method with experimental results of Deere's work (2000) at a selected condition. At wide range working conditions of critical parameters, e.g. NPR, SPR, Ma number, the predicted results on vector performance and thrust coefficient by a chosen turbulence model may have a little different from experimental results, due to the simulation ability on flow separation under negative pressure gradient and shock wave / boundary layer interactions. But we believe the deviation would not have significant influences on quantitative results and qualitative regularity, and the judgment could be confirmed by the later experimental work.

4. CONCLUSION

The flow characteristics and vector performance (vector angle and thrust coefficient) comparison on

2D and axisymmetric SVC nozzles were investigated numerically. The affecting factors including nozzle pressure ratio (NPR), secondary pressure ratio (SPR) and free stream Ma number (M_∞) were considered, and conclusions can be drawn as follow.

1) The unbalanced pressure distribution on nozzle walls induced by secondary injection is the dominating factor for primary flow deflecting, while the shock wave is responsible for thrust loss which is about a reduction of 6%-12% on thrust coefficient. Compared with flow characteristics a 2D SVC nozzle, free restriction of the injection slot of an axisymmetric SVC nozzle changes the configurations of vortices and caused the pressure release between high pressure zone upstream of injection slot and low pressure zone downstream of injection slot.

2) Under smaller NPR, the pressure release mechanism of an axisymmetric SVC nozzle causes vector angle (δ_p) smaller, and it is about 16.5% less than that of a 2D SVC nozzle at NPR of 6, while there is tiny difference δ_p at NPR of 13.88 and 16. When SPR excesses 1.2, the induced shock wave interacts with the upper wall of a 2D SVC nozzle and results in 12% smaller of δ_p than that of an axisymmetric SVC nozzle at SPR of 1.5; meanwhile the thrust coefficient (C_{fg}) of a 2D SVC nozzle is smaller within 1.2%. The unbalanced pressure distribution on SVC nozzle outer walls caused by free stream weakens vector performance, and its influence on a 2D SVC nozzle is more obvious, especially under transonic condition of M_∞ of 0.9 and 1.1, at which condition the δ_p of a 2D SVC nozzle is 11.2% smaller than that of an axisymmetric SVC nozzle; the variation of C_{fg} with M_∞ is within 0.2%, and the C_{fg} of an axisymmetric SVC nozzle is about 0.8% larger than that of a 2D SVC nozzle.

Other research work would be carried out in the future, e.g. investigation of the comparison on after-body penalty, installment performance and infrared radiation characters for 2D and axisymmetric SVC nozzles, which could help to understand the comprehensive performance of this kind of fluidic thrust vectoring technology.

ACKNOWLEDGEMENTS

REFERENCES

Anderson, C. J., V. J. Giuliano and D. J. Wing (1997). Investigation of hybrid fluidic/ mechanical thrust vectoring for fixed exit exhaust nozzle. AIAA 97-3148.

Bellandi, E. G. and A. J. Slippey (2009). Preliminay analysis and design enhancements of a dual throat FTV nozzle concept. AIAA 2009-3900.

Catt, J. A. and D. N. Miller (1995). A static investigation of fixed geometry nozzles using fluidic injection for throat area control. AIAA 95-2604.

Chai, X. C (2012). Numerical simulation of high speed turbulent jets in crossflow. Ph. D. Thesis, The university of Minnesota.

Chiarelli, C., R. K. Johnsen and C. F. Shieh (1993). Fluidic scale model multi-plane thruat vector control test results. AIAA 93-2433.

Deere, K. A (2000). Computatonal investigation of the aerodynamics effects on fluidic thrust vectoring. AIAA 2000-3598.

Deere, K. A. (2003). Summary of fluidic thrust vectoring research conducted at NASA Langley Research Center. AIAA 2003-3800.

Deere, K. A., B. L. Berrier and J. D. Flamm (2005). A computational study of a new dual throat fluidic thrust vectoring nozzle concept. AIAA-2005-3502.

Federspiel, J. and L. Bangert (1995). Fluidic control of nozzle flow- some performance measurements. AIAA 95-2605.

Ferlauto, M. and R. Marsilio (2016). Open and closed-loop responses of a dual throat nozzle during fluidic thrust vectoring. *Propulsion and Energy Forum, July 25-27, 2016, Salt Lake City, UT*, AIAA 2016-4504.

Giuliano, V. J., T. H. Flugsrad and *et al.* (1994). Static investigation and computational fluid dynamics (CFD) analysis of flow path cross-section and trailing-edge shape variations in to multi-axis thrust vectoring nozzle concepts. AIAA 94-3367.

Gu, R. and J. L. Xu (2015). Dynamic experimental investigations of a bypass dual throat nozzle. *Journal of Engineering for Gas Turbines and Power* 136(8), 084501-6.

Hamed, A. and G. Laskowski (1997). A parametric study of slot injection thrust vectoring in a 2DCD nozzle. AIAA 1997-3154.

He, C. J., J. Q. LI and Y. H., LI (2017). Influence of secondary injection parameters on performance of shock vector control nozzle. *International Space Planes and Hypersonic Systems and Technologies Conference,* 6-9 March 2017, Xiamen China, AIAA 2017-2270,

Heo, J. Y. and H. G. SUNG (2012). Fluidic thrust-vector control of supersonic jet using coflow injection. *Journal of Propulsion and Power* 28(4), 858-861.

Liu. Z. M., C. CHEN and F.SHEN (2014). Impact of Ma number of external flow on performance of counterflow thrust vectoring nozzle. *Journal*

of Propulsion Technology. 35(3), 442-448.

Mason, M. S. and W. J. Crowther (2004). Fluidic thrust vectoring for low observable air vehicle. AIAA 2004-2210.

Miller, D. N., P. J. Yagle and J. W. Hamstra (1999). Fluidic throat skewing for thrust vectoring in fixed geometry nozzles. AIAA 99-16262.

Saghafi, F. and A. Banazadeh (2006). Co-flow fluidic thrust vectoring requirements for longitudinal and lateral trim purposes. AIAA 2006-4980.

Scharnhorst, R. K. (2013). Characteristics of future military aircraft propulsion systems. AIAA 2013-0466.

Sehra, A. K. and W. Jr. Whitlow (2004). Propulsion and power for 21st century aviation. *Progress in aerospace sciences* 40, 199-235.

Shi, J. W., Z. X. Wang, X. B. Zhang and Z. W. Liu (2013). Study on counter-flow thrust vectoring nozzle jet attachment and control. *ACTA AERODYNAMICA SINICA* . 31(6), 723-726.

Shi, J. W., Z. X. Wang, X. B. Zhang and Z. W. Liu (2013). Effects of secondary injection forms on vector performance of shock vectoring nozzle. *Journal of aerospace power* 28(12), 2678-2684.

Shih, C., F. S. Alvi and D. M. Washington (1999). Effects of counter-flow on the aeroacoustic properties of s supersonic jet. *Journal of aircraft* 36(2), 451-457.

Sriram, A. T. and J. Mathew (2004). Numercal prediction of two-dimensional transverse injection flows. AIAA 2004-1099.

Strykowski, P. J. and A. Krothapalli (1993). The Countercurrent Mixing Layer: Strategies for Shear-Layer Control. *AIAA 3rd Shear Flow Control Conference, July 1993.*

Terrier, D. A. and F. K. Lu (2003). Aerodynamically controlled expansion nozzle for STOVL aircraft. AIAA 2003-185.

Waithe, K. A. and K. A. Deere (2003). Experimental and computational investigation of multiple injection ports in a convergent-divergent nozzle for fluidic thrust vectoring. AIAA 2003-3802.

Wing, D. J. (1994). Static investigation of two fluidic thrust vectoring concepts on a two-dimensional convergent-divergent nozzle. NASA TM-4574.

Yagle, P. J., D. N. Miller and K. B. Ginn (2001). Demonstration of fluidic throat skewing for thrust vectoring. *Transaction of the ASME Journal of Engineering for Gas Turbines and Power* 123(3), 502-507.

Zhang, J. D. and Z. X. Wang (2012). Numerical research on two types of fluidic thrust vector. *Acta aerodyanmica sinica* 30(2), 205-209.

Zmijanovic, V., V. Lago, M. Sellam and *et al*. (2014). Thrust shock vector control of an axisymmetric conical supersonic nozzle via secondary transverse gas injection. *Shock Wave*, 24, 97-111.

Zmijanovic, V., L. Leger and V. Lago (2012). Effects of the inlet gases thermodynamic properties on a fluidically thrust vectorized supersonic nozzle. *18th AIAA/3AF International Space Planes and Hypersonic Systems and Technologies Conference 24-28 September 2012, Tours, France,* AIAA 2012-5932.

Zukoski, E. E. and E. W. Spaid (1964). Secondary injection of gases into supersonic flow. *AIAA Journal*, 2, 1689-1696.